Presented at Algorithms for Multispectral & Hyperspectral Imagery (SPIE Vol. 3717),
Aerosense 99, Orlando, FL, April 5-9, 1999

Subpixel temperature retrieval with multispectral sensors

John J. Szymanski,* Christoph C. Borel, Quincy O. Harberger,
Pawel Smolarkiewicz and James Theiler

Los Alamos National Laboratory, Space and Remote Sensing Sciences Group,
Mail Stop C323, Los Alamos, NM 87545

ABSTRACT

High-quality, multispectral thermal infrared sensors can, under certain conditions, be used to measure more than one surface temperature in a single pixel. Surface temperature retrieval in general is a difficult task, because even for a single unknown surface, the problem is under-determined. For the example of an N-band sensor, a pixel with two materials at two temperatures will, in principle, have 2(N+1) unknowns (N emissivities and one temperature for each of two materials). In addition, the upwelling path and reflected downwelling radiances must be considered. Split-window (two or more bands) and multi-look (two or more images of the same scene) techniques provide additional information that can be used to reduce the uncertainties in temperature retrieval. Further reduction in the uncertainties is made if the emissivities are known, either a priori (e.g., for water) or by ancillary measurements. Ultimately, if the number of unknowns is reduced sufficiently, the performance of the sensor will determine the achievable temperature sensitivity. This paper will explore the temperature sensitivity for a pixel with two temperatures that can be obtained under various assumptions of sensor performance, atmospheric conditions, number of bands, number of looks, surface emissivity knowledge, and surface composition. Results on synthetic data sets will be presented.

Key words: Subpixel analysis, multispectral analysis, temperature measurements, thermal infrared

1. INTRODUCTION AND GOALS

The multispectral information available from modern thermal infrared sensors (e.g., ASTER or MODIS) can be, under certain conditions, used to measure more than one surface temperature in a single pixel. This information can be used in water-only pixels to pick out the edges of a thermal plume or, potentially, to retrieve water temperature for mixed land-water pixels. The latter is particularly useful for narrow water channels, where a significant portion of the water surface is contained in mixed land-water pixels (see Fig. 1). All shoreline pixels are necessarily composed of land and water – thus subpixel temperature retrieval can be used to measure water temperatures on shorelines or for smaller bodies of water. The fraction of shoreline pixels obviously increases for instruments with larger ground-sample distances.

This paper describes a method to extract temperatures for materials that occupy less than a full pixel. The present results are for simulated scenes and no atmospheric effects are included (although a method is outlined for providing the corrections). The method requires reasonable knowledge of water and land emissivities and an independent means of measuring the areal fractions of each pixel occupied by the two materials (the sensors discussed below can measure the areal fractions with other bands). The sensitivity of the results to detector noise and calibration error is presented.

Studies of fire or volcanic plume temperatures have been undertaken by Green (1996), Oppenheimer et al. (1993), and Prins & Menzel (1992). The first two papers use the Airborne Visible/Infrared Imaging Spectrometer (AVIRIS) to study biomass fires and volcanic hot spots, respectively. The third paper uses the Visible Infrared Spin Scan Radiometer Atmospheric Sounder (VAS) to study biomass fires. These papers present methods to measure relatively high fire temperatures in hyperspectral data extending to 2.5 μm (the first two) or with a thermal infrared multispectral sensor (the latter paper). In contrast, this paper explores the possibility of measuring temperatures of two materials near 300 K using multispectral thermal infrared data, with emphasis on temperature retrieval accuracy. An important feature of the present method is that other bands within the sensor are used to determine the areal fractions each material occupies with the goal of reducing overall temperature errors (the papers cited above outline methods that attempt to retrieve the fractions and temperatures simultaneously). Dozier (1981) uses multispectral data to retrieve temperatures and areal fractions from multiple pixels. The present method is suitable for a single pixel, although data from multiple-pixels would be used for atmospheric corrections.

*Correspondence: Email: szymanski@lanl.gov; Telephone: 505 665 9371; Fax: 505 667 3815

A complimentary technique was described by Bellerby et al. (1998), who used microwaves to measure brightness temperatures from coastal mixed land-water pixels.

2. SCIENTIFIC BASIS

Retrieving even one temperature per pixel is a difficult task. In the case of a uniform pixel at a single surface temperature, the radiance measured at the top of the atmosphere (TOA) in a thermal infrared (TIR) band *i* is

$$L^i_{TOA} = \varepsilon^i B^i(T_{surface})\tau^i_{atm} + L^i_{upwelling} + L^i_{downwelling}(1-\varepsilon^i)\tau^i_{atm} \quad , \tag{1}$$

where ε^i is the emissivity in the band *i*, B^i is the Planck function averaged over band *i*, $T_{surface}$ is the surface temperature (the goal of the measurement), τ^i_{atm} is the atmospheric transmission in band *i*, and the last two terms are the upwelling and reflected downwelling radiances in band *i*. The basic problem is that there are *N* measurements, but at least *N*+1 unknowns (the N ε^i emissivities and one temperature, $T_{surface}$). Furthermore, in a mixed pixel there are in principle 2(*N*+1) unknowns. This ignores the unknown atmospheric state's effect on the upwelling and downwelling radiances. In the case of a water temperature retrieval, the emissivities are known, and $T_{surface}$ can be robustly retrieved (see Borel et al. (1999)).

Often there are several additional pieces of information that can be used, such as multiple looks at a given scene (nadir and some other angle). Information from these multiple looks can be used to eliminate some atmospheric effects. Also, day and night image acquisition allows one to look at the same scene under different thermal conditions (well into the night, the temperature difference between materials with different emissivities may reverse from its daytime bias). In the case of ASTER and MODIS, one can take advantage of images acquired in the visible and near IR (VNIR) that have a 4x or 6x smaller ground-sample distance. These images can be used to identify mixed TIR pixels and measure the fractions of a mixed pixel that are different surface types (e.g., define a land-water boundary). Clearly this problem is difficult enough without considering more than two temperatures per pixel. Thus, two cases will be considered in this paper:

1. Retrieving temperatures from a pixel containing two materials with substantially different, but known, emissivities. Most of the results in this paper are for this case.

2. Retrieving temperatures from a pixel with a single material at two different temperatures (for example, a pixel that is homogenous in composition, but partially in shadow, or a thermal plume in water).

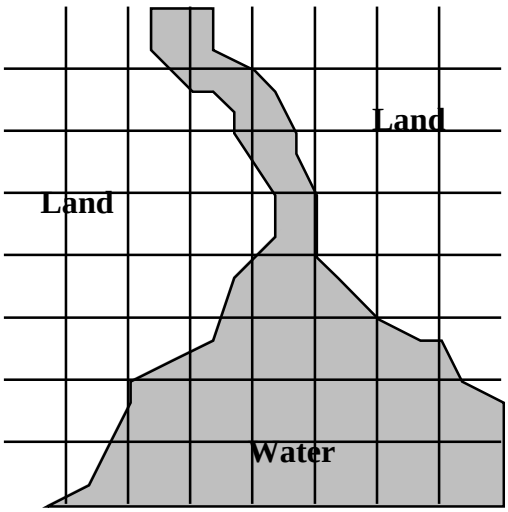

Figure 1. Pixels superimposed on a scene. Note that the land-water mixed pixels have many different water fractions.

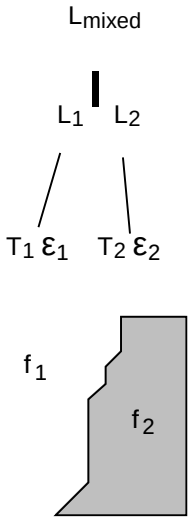

Figure 2. The definition of a mixed pixel in terms of areal fractions, temperatures, emissivities, and radiances.

3. THE PHYSICAL MODEL

3.1 The radiance from a mixed pixel

The top-of-the-atmosphere (TOA) radiance emitted by a mixed pixel in band *i* is (assuming the independent-pixel approximation, i.e., no coupling between the subpixels, which is a very good approximation in the TIR)

$$L^i_{mixed} = \left(f_1 \varepsilon^i_1 B^i(T_1) + f_2 \varepsilon^i_2 B^i(T_2)\right)\tau^i_{atm} + L^i_{upwelling} + L^i_{downwelling}(r^i)\tau^i_{atm}, \quad (2)$$

where r^i is the reflectance of the mixed pixel, f_1 and f_2 are the areal fractions of the pixel that are at temperatures T_1 and T_2, respectively, τ^i_{atm} is the atmospheric transmission, the ε's are emissivities, and the B's are band-averaged Planck functions (see Fig. 2). Note that the temperatures, emissivities, and atmospheric transmissions are effective values because of band-averaging. Reflected, downwelling radiance will be a small effect for high-emissivity natural surfaces and will be ignored here. If the emissivities are known with some error and the fractions f_1 and f_2 can be determined from spatial cues in the visible or input by a data analyst, then there remain 2N+2 unknowns (the upwelling radiances and atmospheric transmissions for each of N bands and 2 temperatures) and the N TIR band measurements. Therefore, some atmospheric model is needed. Upwelling radiance and atmospheric transmission can be parameterized for the five TIR bands as a function of columnar water (CW) and effective atmospheric temperature T_{atm_eff}. A consistent set (i.e., a set that produces smooth temperature values) of the *CW* and T_{atm_eff} values can be produced using a physics-based temperature retrieval (Borel (1999)). The physics-based temperature retrieval would be applied over a set of pixels that are believed to have a single, uniform temperature. Thus, if the C*W* and T_{atm_eff} are determined from an independent set of pixels in the same scene, the 2N+2 unknowns are reduced to the two temperatures, with radiance measurements in N bands. Further atmospheric information from a multiple-look maneuver could also be used.

With the approximation outlined above, the measured radiance from a mixed pixel is

$$L^i_{mixed} = \left(f_1 \varepsilon^i_1 B^i(T_1) + f_2 \varepsilon^i_2 B^i(T_2)\right)\tau^i_{atm}(CW) + B^i\left(T_{atm\_eff}\right)\left(1 - \tau^i_{atm}(CW)\right) . \quad (3)$$

In this model τ^i_{atm} is a function of columnar water (CW) and the second term has been substituted for the upwelling radiance. Using the *CW* and T_{atm_eff} values from the physics-based temperature retrieval, a new quantity is defined

$$L^i_{reduced} = \left(L^i_{mixed} - B^i\left(T_{atm\_eff}\right)\left(1 - \tau^i_{atm}(CW)\right)\right) \Big/ \tau^i_{atm}(CW) = f_1 \varepsilon^i_1 B^i(T_1) + f_2 \varepsilon^i_2 B^i(T_2) , \quad (4)$$

which can be fit for T_1 and T_2, given some knowledge of the emissivities and the fractions f_1 and f_2. Note that the fit is easier if the two emissivities are not equal, provided they are known, because there is more structure from band-to-band to separate the two terms in equation 4. The algorithm outlined here is illustrated in Fig. 3. As an aside, an alternative approach may be useful, which is to introduce the concept of "virtual cold", developed by Gillespie et al. (1990), to further aid in the unmixing.

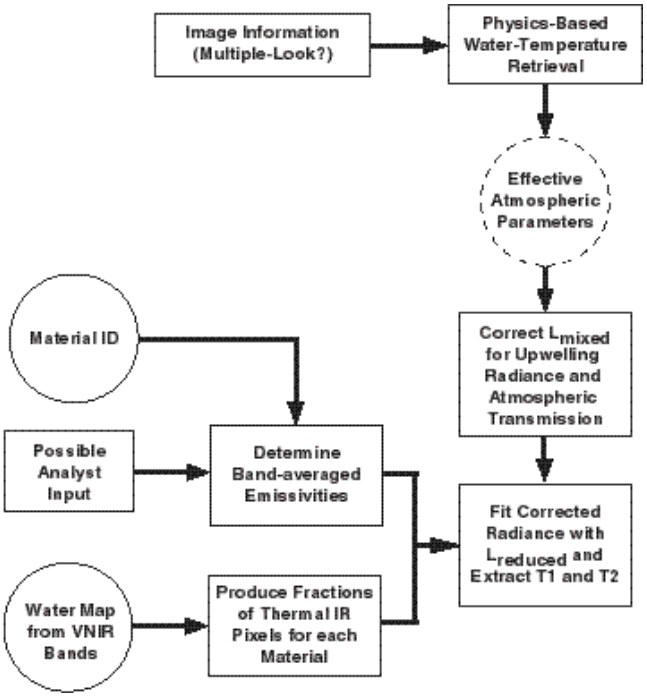

Figure 3. Subpixel temperature retrieval algorithm.

3.2 Modeling results

To test these ideas, scenes with mixed land-water pixels were simulated. Atmospheric effects were not included in this simulation. A synthetic river scene was created with riverbank pixels that are partly land and partly water (see Fig. 4). The radiance, $L_{reduced}$ from mixed pixels in the scene was modeled with equation 4. Smearing due to the detector noise, calibration errors, emissivity uncertainties and/or areal fraction errors was added. All errors are uncorrelated and enter into the simulation identically. Calibration errors and detector noise were added at typical levels according to the ASTER and MODIS specifications and some hypothetical cases (MODIS, 1999; ASTER 1999; Gillespie, 1996). The ASTER and MODIS thermal infrared bands used in the analysis are shown in Tables 1 and 2, respectively. If the VNIR bands have a 4x smaller ground-sample distance (GSD), then the pixel area is 16x smaller (~6%). Thus, an areal fraction error of ±3% rms is used in this analysis (ASTER has 6x smaller VNIR GSD and, therefore, a somewhat smaller areal fraction error). The water emissivities in all spectral bands are assumed to be well-known and are assigned no error. This last assumption in effect limits the method to water surfaces in the presence of low wind speeds, as the emissivity change with surface roughness is not taken into account. Land emissivity uncertainties are included by retrieving the temperature using the average emissivity of eight different soil types from the Salisbury (Salisbury and D'Aria, 1992) database. The TOA radiance from each pixel is simulated by randomly choosing among the eight soil types. No vegetation was included in the simulations.

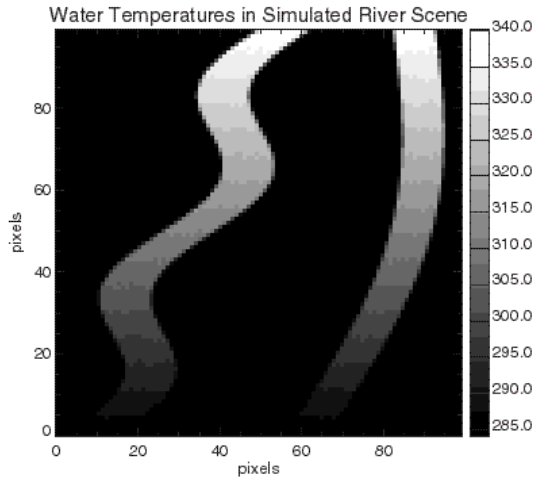

Figure 4. Simulated river scene. The water temperature scale is shown on the right (in K). The land temperature is uniformly 285 K. The pixels analyzed are located along the river shorelines, corresponding to mixed land-water pixels.

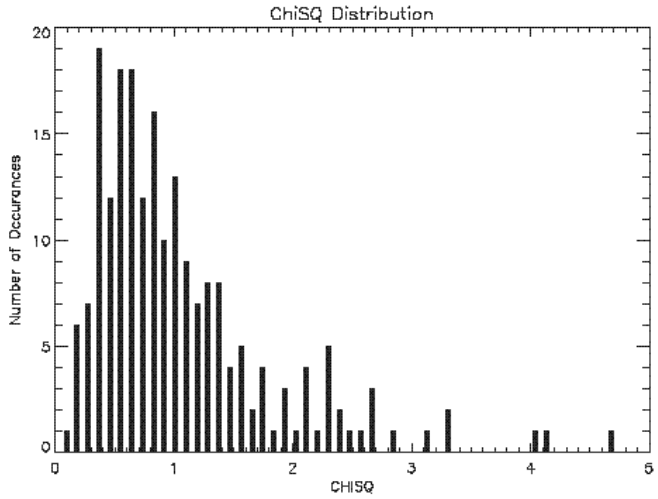

Figure 5. Chi-squared distribution for all the mixed-pixel fits in a single simulated river scene (for the MODIS sensor with detector noise of 1.5% and SNR of 200).

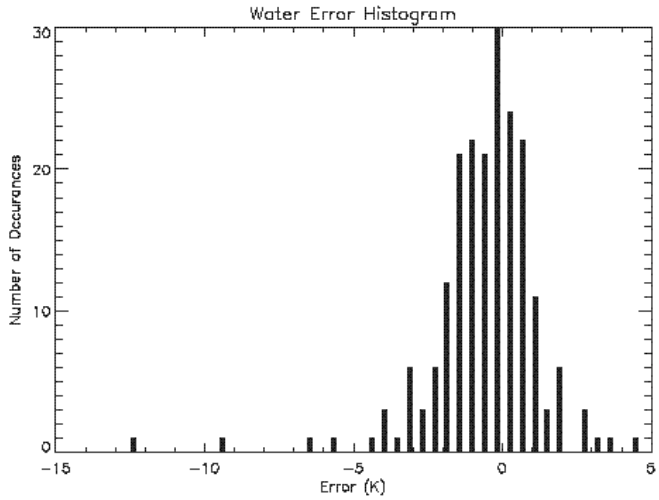

Figure 6. Distribution of errors in the water-temperature retrieval for mixed land-water pixels. This histogram is for the same scene described in Fig. 5.

Table 1. The ASTER thermal infrared bands. All of these bands were used in the simulations (ASTER, 1999).

ASTER Thermal IR Bands	
Band	**Wavelengths (μm)**
10	8.125 – 8.475
11	8.475 – 8.825
12	8.925 – 9.275
13	10.25 – 10.95
14	10.95 – 11.65

The simulated radiances in multiple bands emitted from mixed pixels in the river scene were fit to $L_{reduced}$. At this point, of course, the original values have errors added and the fit will not be exact. Pixels within the scene are categorized according to what fraction of each is water. Water temperatures will be the emphasis of this work, so pixels with less than 30% water were not considered. Pixels containing more than 90% water are not considered mixed pixels and are not a part of these results. Thus, pixels analyzed are 30%-90% water and 10%-70% land, and the results for land temperatures are necessarily worse than for water temperatures.

Typical fit results are illustrated in Figs. 5 and 6. Fig. 5 shows the chi-squared distribution for a series of fits of $L_{reduced}$ to approximately 100 mixed pixels in the river scene. Fig. 6 shows the output temperature error distributions for the same simulation. Note that the results discussed below

Table 2. The MODIS thermal infrared bands. All these bands were used in the simulations (MODIS, 1999).

MODIS Thermal IR Bands					
Band	**Wavelengths (μm)**	**Band**	**Wavelengths (μm)**	**Band**	**Wavelengths (μm)**
20	3.660 - 3.840	27	6.535 – 6.895	32	11.770 – 12.270
21	3.929 – 3.989	28	7.175 – 7.475	33	13.185 – 13.485
23	4.020 – 4.080	29	8.400 – 8.700	34	13.485 – 13.785
24	4.433 – 4.498	30	9.580 – 9.880	35	13.785 – 14.085
25	4.482 – 4.549	31	10.780 – 11.280	36	14.085 – 14.385

should be considered representative, with the trends being significant, and the temperature results being reliable to 10-20%. In other words, because of the random inputs used to simulate statistical errors, if the same scene is simulated 10 times, the resulting rms temperature error will vary by 10-20%.

Results for the ASTER and MODIS sensors were obtained by utilizing approximate values for calibration error and detector noise in the simulation and analysis (MODIS, 1999; ASTER 1999; Gillespie, 1996). The results for the ASTER sensor are in Table 3. It should be noted that the ASTER sensor was not designed for this type of retrieval, and whole-pixel temperature retrievals, including the difficult land temperature-emissivity separation, are expected to be very accurate (~1.5 K, Gillespie, 1996). Better results for subpixel temperature retrieval are achieved if a hypothetical mid-wave infrared (MWIR) band were added to the existing long-wave infrared (LWIR) bands in the ASTER sensor. A 'typical' MWIR band located from 3.66 µm to 4.08 µm was added to the simulation, with results shown in the last two lines of Table 3. Because both the SNR and calibration errors are expected to be substantially worse in the MWIR, the last row is the most representative result. No reflected sunlight was added to the simulation, corresponding to a nighttime retrieval (the standard ASTER temperature retrievals work during day or night).

It is clear that even a single MWIR band provides substantially improved accuracy for subpixel temperature-retrieval. This is no surprise, because the change in radiance for a given temperature change is much larger for a MWIR band than a LWIR band (recall that for particularly low temperatures, a band at the shortest wavelengths would register little or no radiance). To illustrate this effect, consider the change in radiance emitted by a blackbody at 270 K vs. 300 K. At 4.0 µm, the radiance is 0.19 w/(m^2-µm-sr) at 270 K and 0.72 w/(m^2-µm-sr) at 300 K for a change of 0.53 w/(m^2-µm-sr), or a radiance ratio of 3.8. At 10.0 µm, the radiance is 5.8 w/(m^2-µm-sr) at 270 K and 9.9 w/(m^2-µm-sr) at 300 K for a change of 4.1 w/(m^2-µm-sr), or a radiance ratio of 1.7. Of course, as pointed out above, the MWIR channels will generally have worse SNR than LWIR channels (InSb MWIR detectors would generally have lower noise than HgCdTe LWIR detectors, but the signal levels in the MWIR are proportionately even smaller). Calibration is also more difficult for the smaller MWIR signal levels. Nevertheless, it appears the MWIR bands are helpful for subpixel temperature retrieval.

Table 3. Nighttime temperature retrieval results for mixed land-water pixels with simulated ASTER sensor data. The rms calibration errors and SNRs are listed for each run. Note that the sensor is not designed for this type of retrieval, hence the last two rows show the results if a hypothetical mid-wave infrared band were added to ASTER.

ASTER Sensor Parameters	RMS Land Temperature Error (K)	RMS Water Temperature Error (K)
1.5% and SNR = 200	27	13
1.0% and SNR = 200	16	12
1.0% and SNR = 300	15	8.3
1.5% and SNR = 200 + MWIR (with 1.5% cal error)	5.0	2.4
1.5% and SNR = 200 + MWIR (with 3% cal error)	6.1	2.8

A similar analysis was performed for the MODIS sensor. Again, approximate values for calibration error and detector noise for the MODIS sensor (MODIS, 1999) were put into the simulation and analyzed, with the results shown in Table 4. If the as-built calibration errors for MODIS are larger than used in this simulation, the results would scale up accordingly (this is particularly likely in the MWIR). By comparing the MODIS results with the ASTER results including the hypothetical MWIR band, it is evident that sensor performance plays some role in the accuracy of the temperature retrieval, but a larger effect is due to the additional shape discrimination provided by one or more MWIR bands. In either case, MODIS is an excellent sensor for subpixel temperature retrieval, because it has many thermal IR bands, good detector noise characteristics, and good calibration accuracy.

Table 4. Nighttime temperature retrieval results for mixed land-water pixels with simulated MODIS sensor data. The rms calibration errors and SNRs are listed for each run. The last row shows the result if the MWIR calibration error and SNR are degraded.

MODIS Sensor Parameters	RMS Land Temperature Error (K)	RMS Water Temperature Error (K)
1.5% and SNR = 200	3.9	1.5
1.0% and SNR = 200	2.8	1.2
1.0% and SNR = 300	2.3	1.1
LWIR: 1.5%; SNR = 200 **MWIR: 3%; SNR = 100**	4.0	2.7

To study the sensitivity of the results to a single source of error, the input value for the calibration error was varied and the fits repeated. The results are shown in Fig. 7, where no emissivity uncertainties or areal fraction errors are included, and the error contribution due to detector noise is negligible. It is clear that any significant uncertainty in the simulated radiances leads to a substantial temperature retrieval error. This is because much of the sensitivity of the fit is due to the shape of the radiance spectrum. The information 'pushing' the fit to the correct temperature is quickly lost, as errors in the radiance are included. In addition, land and water temperatures can compensate each other, with a higher land temperature somewhat compensating for a too-low water temperature. This compensation is most effective when the emissivities are similar - the larger the difference, the more difficult it is for the compensation to occur. These effects are further illustrated in Table 5, where the effect of turning on the various sources of error is shown.

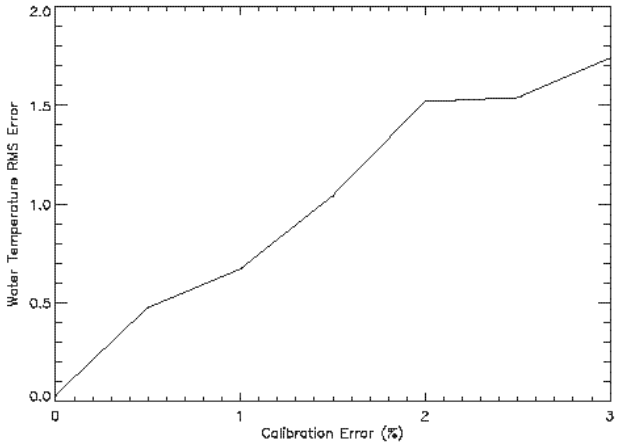

Figure 7. This plot shows the onset of the rms temperature error as the calibration error is increased from zero. All other sources of error are zero in this plot. Results are for the MODIS sensor under the same conditions shown in figures 5 and 6.

Table 5. Nighttime temperature retrieval results for mixed land-water pixels with simulated ASTER sensor data. These results are for the ASTER sensor with hypothetical mid-wave infrared band added. The rms calibration errors are 1.5% and SNRs are 200. Emissivity and areal fraction errors are described in the text. Each succeeding line has an additional source of error added to the simulation.

Errors Included	RMS Land Temperature Error (K)	RMS Water Temperature Error (K)
None	0.03	0.02
SNR	1.8	0.5
SNR, cal. error	2.4	1.1
SNR, cal. , and areal fraction errors	4.0	1.4
SNR, cal. , areal fraction, and emissivity errors	5.0	2.4

3.3 A single material at two different temperatures

What can be done in the other situation, where a pixel contains a single material that is at two different temperatures? Conceptually, one can consider extracting two temperatures in this situation, although the task is considerably tougher than in the situation discussed above. The governing hypothesis in this section is that the radiance produced in the thermal bands from two Planck functions, L_{mixed}, is distinguishable, within errors, from the radiance produced by a single Planck function (i.e., the radiance that would be produced by an entire pixel at a single temperature). If these two situations can't be distinguished, then there is no chance of retrieving two separate temperatures. The extent to which this hypothesis is fulfilled sets the limits of the method. Note that a single material at two temperatures would generally have a gradient of temperatures between the high and low values. Because the pixels are large in the instruments considered here, a temperature gradient over, for example, 10 meters would behave as an abrupt temperature change between two sharply-defined subpixels.

It is instructive to study the radiance as a function of wavelength for two situations: (1) a mixed pixel whose radiance is described by two Planck functions at two temperatures (simulated using equation 2 with emissivities = 1.0 and no atmospheric effects included) and (2) a single Planck function representing the radiance one expects if the pixel were pure. The temperature used in the single Planck function is a straight average of the brightness temperatures in the TIR bands. The calculations are done using graybodies, so emissivity variation with waveband was ignored. To further accentuate the differences between pure and mixed pixels, take these ratios

$$R_{mixed} = L_{mixed}^{long} \Big/ L_{mixed}^{mid} \qquad R_{pure} = L_{pure}^{long} \Big/ L_{pure}^{mid} \quad , \tag{5}$$

where ‘long’ and ‘mid’ refer to LWIR and MWIR bands, respectively. Ultimately, the measurement errors in R_{mixed} must be smaller than the difference

$$D = \left| 1 - \frac{R_{mixed}}{R_{pure}} \right| . \tag{6}$$

Using MODIS bands 20 (3.66 – 3.84 μm; the shortest wavelength MWIR band) and 31 (10.78 – 11.28 μm; a LWIR band near the peak of the Planck function for terrestrial temperatures), $f_1 = f_2 = 0.5$, $T_1 = 300$K, and $T_2 = 280$K, $R_{\text{mixed}} = 25.8$, $R_{\text{pure}} = 27.9$, and $D = 7.4\%$.

Can $D = 7.4\%$ be detected with MODIS? Assume the SNRs for these two bands are 200 and make the very important assumption that the relative calibration of the MWIR and LWIR bands is 0.5%. In this case, the error on $R_{\text{mixed}} = 1.4\%$. Thus, a mixed pixel with two temperatures of 300 K and 280 K has an observable deviation from the radiances observed

from a single Planck function. Note that no explicit reference has been made to a specific material, but it is assumed that the emissivities are known and uniform within the pixel. Of course, many other sources of uncertainty are not considered, including atmospheric effects, and no estimate of the temperature retrieval errors have been made.

4. DISCUSSION AND SUMMARY

This paper discusses the information and assumptions needed to extract temperatures from pixels containing two materials at two temperatures. This is a difficult problem that requires substantial prior information (the emissivities) and information from other bands in the sensor (to determine areal fractions). Good sensor performance, including low detector noise and good calibration, is critical in determining the ultimate subpixel temperature accuracy. It also appears that MWIR bands are very important to improve the sensitivity of subpixel temperature measurements.

The results from these analyses are quite intriguing, although far from comprehensive. It is difficult to include in simulated data all the effects encountered in real experiments, and, furthermore, these simulations have room for further refinement (including atmospheric effects, for example). Nevertheless, these simulations suggest that it is possible to extract temperatures from mixed pixels, given the quality of modern sensors coming online.

REFERENCES

ASTER instrument specifications, http://asterweb.jpl.nasa.gov/asterhome/instrument.html, accessed February 1999.

Borel, C.C., W.B. Clodius, J.J. Szymanski, and J. Theiler, 1999: "Comparing robust and physically based sea surface temperature retrievals for high resolution, multispectral thermal sensors using one or multiple looks" in this volume.

Bellerby, T., M. Taberner, A. Wilmshurst, M. Beaumont, E. Barrett, J. Scott, and C. Durbin, 1998: "Retrieval of land and sea brightness temperatures from mixed coastal pixels in passive microwave data," IEEE Trans. Geoscience and Remote Sens., **36**, 1844 - 1851.

Dozier, J., 1981: "A method for satellite identification of surface temperature fields of subpixel resolution," *Remote Sens. Environ.*, **11**, 221 - 229.

Gillespie, A.R., M.O. Smith, J.B. Adams, and S.C. Willis, 1990: in proceedings of the TIMS workshop.

Gillespie, A.R., S. Rokugawa, S.J. Hook, T. Matsunaga, and A.B. Kahle, 1996: "Temperature/emissivity separation algorithm theoretical basis document, version 2.3," from the ASTER web site cited above.

Green, R., 1996: "Estimation of biomass fire temperature and areal extent form calibrated AVIRIS spectra," Proceedings of the 1996 AVIRIS Workshop.

MODIS instrument specifications, http://ltpwww.gsfc.nasa.gov/MODIS/MODIS.html, accessed February 1999.

Oppenheimer, C., D.A. Rothery, D.C. Pieri, M.J. Abrams, V. Carrere, 1993: "Analysis of airborne visible infrared imaging spectrometer (AVIRIS) data of volcanic hot spots," *Intl. Journal of Remote Sens.*, **14**, 2919 - 2934.

Prins, E.M., W.P. Menzel, 1992: "Geostationary satellite detection of biomass burning in South America," *Intl. Journal of Remote Sens.*, **13**, 2783 - 2799.

Salisbury, J. W. and D. M. D'Aria, 1992: "Emissivity of terrestrial materials in the 8-14 μm atmospheric window," *Remote Sens. Environ.*, **42**, 83 - 106.